Published in IET Microwaves, Antennas & Propagation
Received on 5th February 2014
Revised on 20th June 2014
Accepted on 15th July 2014
doi: 10.1049/iet-map.2013.0721

Special Issue on Emerging Integrated Reconfigurable Antenna Technologies

ISSN 1751-8725

Phase-steered fixed beams in one and two-dimensional scan space for substrate-integrated radar and radio systems at 60 GHz

Ajay Babu Guntupalli, Ke Wu

Electrical Engineering Department, Poly-Grames Research Centre, Ecole Polytechnique of Montreal, Montreal, Quebec, Canada H3T 1J4
E-mail: ajay-babu.guntupalli@polymtl.ca

Abstract: In this work, one-dimensional (1D) and 2D scan phased array antennas for 60 GHz radio communication and radar sensing systems are proposed, studied and experimentally validated in the substrate-integrated waveguide technology. A linearly polarised phased array with 1D scanned beams in the first part of this study and a right-hand circularly polarised (CP) array with 2D scanned beams in the second part are presented and discussed in detail. In the demonstrated 1D phased array, dielectric rod antenna is used as radiating elements to form 1×4 linear array and then a planar Butler matrix is integrated along with the array to obtain phase-steered beams. In the 2D phased array, CP radiating elements are used to form 2×4 array and then a folded Butler matrix is used to feed the CP array. Simulated and measured characteristics of these two phased array antenna radiation parameters are compared. The proposed phased arrays can be integrated into 60 GHz and other millimetre-wave radar and radio systems as an integrated antenna front-end.

1 Introduction

Reconfigurable and smart antennas with electronically steerable beams have numerous advantages and applications in wireless data communication, microwave power transmission and automotive radar sensing. These antennas are highly desired for many performance-enhanced platforms over a wide range of radio frequencies from commercial cellular bands up to terahertz range. Cognitive radio antenna front-end should meet a multitude of requirements such as the re-configurability of beam direction, polarisation and frequency bandwidth [1–4]. Phased array antenna with one-dimensional (1D) and 2D scanning patterns presents numerous applications depending on the related cognitive radio or radar front-end requirements. 1D scan system can have phase-controlled beams only in one direction where a linear phase gradient is varied along the array input contour [5]. A beamforming network (BFN) driven linear array involves more freedom, which can be fed from an edge of array. In 2D scan systems, phase-controlled beams are scanning in azimuth and elevation planes [5]. The selection of a BFN is, nevertheless, critical in such 2D scan systems because of the phase gradients varied along the two directions. At millimetre-wave (mm-wave) frequency, the selection of substrate-integrated waveguide (SIW) in the design and development of a BFN topology has proven to be excellent [6].

2D scanning can be obtained by phase controlling an array of leaky wave sources where phase shifters are used for the azimuth plane scanning, and frequency-scanning property is used for the elevation plane scanning [7]. However, many antenna front-end applications require a fixed outgoing beam in the operating frequency range. 2D scanning using phase only techniques have been studied in [8–12]. Low temperature co-fired ceramic technology (LTCC) in [8], microstrip feeding network in [9] and low-cost SIW technology have been all used to reconfigure the beam direction using phase only technique in [10–12]. The SIW feeding antenna arrays were realised on a silicon substrate to implement system on chip [13]. Advances in silicon technology allow the realisation of low-cost radiofrequency (RF) front-end solutions [14]. In [15], a planar SIW fed slot array antenna was proposed and its array efficiency was measured to be 68% at 60 GHz. However, inherent narrow-band nature of the slotted waveguide structure limits its impedance bandwidth and the deployed series feeding method creates a hurdle for the pattern bandwidth. The present work, which comes up with a planar dielectric rod antenna solution, resolves those problems and presents a full-planar structure with wideband impedance and radiation pattern bandwidth.

Dielectric rod antenna has inherent and well-documented advantages such as simple architecture, wide impedance bandwidth and high radiation efficiency [16–23]. In particular, the planar nature of certain dielectric rod antenna techniques allows their integration along with millimetre-wave integrated circuits onto a single platform. The inherent wideband nature of rod antenna was used for the realisation of compact ultra-wideband sensor [16] and

ground penetrating radar system [18]. For planar antennas, feeding can be implemented in the microstrip technology or SIW technology. SIW-enabled anti-podal linearly tapered slot array (ALTSA) has been proposed in [21–23]. Antenna developed in [24] was a corrugated ALTSA loaded with an elliptical shaped dielectric, a large aperture will not be suitable for implementing low side-lobe level (SLL) antenna arrays. In this work, a technique is proposed to decrease the aperture size of rod antenna and to improve pattern bandwidth, aiming to implement a compact and high gain antenna array.

This paper is organised as follows. The physical mechanism of dielectric rod antenna is described in Section 2. 1D scan phased array developed on the basis of a 1×4 rod antenna array is discussed in Section 3. The right-hand circularly polarised (RHCP) phased array with 2D scanned beam patterns is discussed in detail in Section 4. Finally, conclusions are drawn in Section 5.

2 Dielectric rod antenna characterisation

In the following, a linearly polarised dielectric rod antenna is proposed over the 60 GHz frequency range and its application in the design of a phased array is also discussed. The dielectric rod antenna is fabricated by using a printed-circuit board (PCB) process on single Rogers 3006 substrate with $\varepsilon_r = 6.3$, $\tan\ \delta = 0.003$ and thickness = 0.635 mm. It is

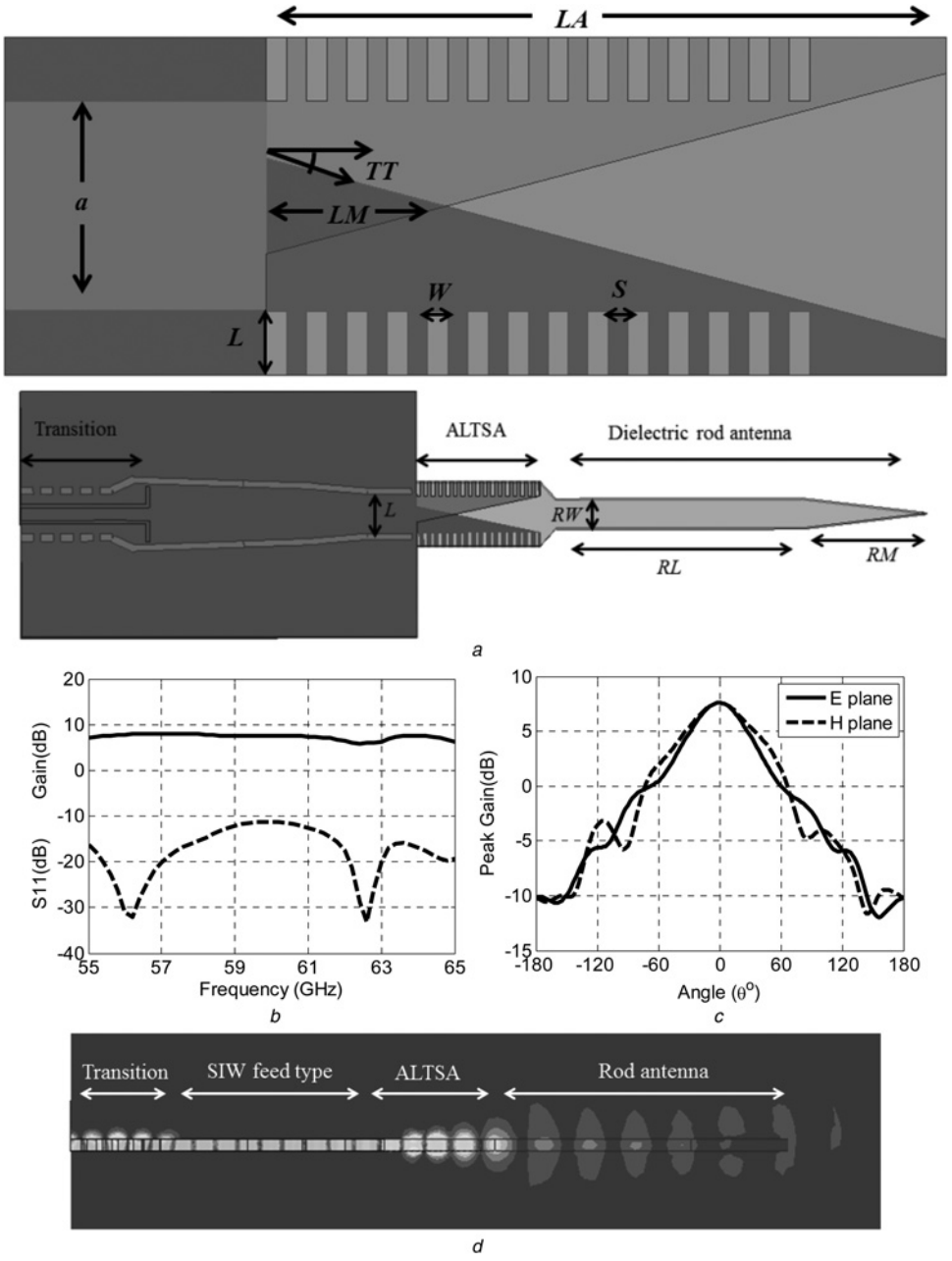

Fig. 1 *ALTSA antenna is initially designed on dielectric substrate*

a ALTSA is loaded by a tapered dielectric rod, $RW = 1.2$, $RL = 10$, $RM = 5$, $L = 1.6$, $LA = 5.1$, $TT = 12°$, $LM = 1.9$, $W = 0.14$, $S = 1.16$ and $a = 1.6$ (where all dimensions are in mm)

b ALTSA antenna impedance matching and gain as a function of frequency

c Simulated radiation behaviour in *E* and *H*-planes at 60 GHz

d Electric field strength inside the dielectric guide

doi: 10.1049/iet-map.2013.0721

theoretically characterised by full-wave electromagnetic software HFSSv14 developed by ANSYS.

2.1 ALTSA antenna architecture

Among the end-fire radiating antenna structures, ALTSA has widely been used in various applications thanks to its simplicity in architecture. Recently, a 60 GHz ALTSA has been proposed in [22] and a radiation behaviour has been obtained over the full band of frequencies from 55 to 67 GHz. Note that the antenna was designed on dielectric substrate (RO 4003) with $\varepsilon_r = 3.38$. As substrate permittivity value increases, most of electrical fields are more concentred inside the dielectric region and radiation efficiency becomes poorer.

As shown in Fig. 1*a*, ALTSA antenna is initially designed on dielectric substrate with $\varepsilon_r = 6.3$. Slots near edge of the ALTSA antenna are corrugated to improve cross-polarisation and to match input impedance. All the physical parameters are optimised to obtain a good radiation pattern performance. Antenna reflection coefficient and gain as a function of frequency are shown in Fig. 1*b*. Magnitude of reflection coefficient with $|S11| \leq -10$ dB is obtained over 16.6% of bandwidth at 60 GHz. Peak gain is better than 6 dBi over the entire desired frequency band.

As shown in Fig. 1*c*, the antenna gain pattern is symmetrical in both *E*- and *H*-planes and half-power beam width (HPBW) is 70°. Simulated cross-polarisation is lower than −15 dB and peak gain is 7.4 dBi only. Antenna input matching condition is a function of geometrical parameters *LM* or *TT*. Parameter *LM* is optimised and set as *LM* = 1.9 mm for the given design. In the ALTSA antenna, gain is known as a function of length *LA*. If *LA* increases, *LM* should be increased. Nevertheless, the antenna impedance cannot be matched over the entire frequency band. For the proposed antenna architecture, electric field is mainly concentrated inside the high permittivity dielectric substrate.

2.2 Rod antenna architecture

To further enhance the gain of ALTSA antenna, a dielectric rod antenna shown in Fig. 1*a* is proposed. In this case, the dielectric rod is loaded at the output end. The rod antenna edge is tapered and length *RM* is chosen to be one-quarter wavelength. The thickness of substrate is chosen to be 0.635 mm, which corresponds to a wider microstrip line. To obtain a better matching condition, a grounded coplanar waveguide (GCPW) to SIW transition is designed and used to measure the cascaded section of ALTSA and rod antenna. The final architecture is a series combination of dipole, linearly tapered slot antenna and dielectric rod antenna. In Fig. 1*d*, the field propagation inside a high-permittivity dielectric substrate is shown at 60 GHz. Each junction is matched to obtain a continuous power flow along the aperture of dielectric rod antenna.

The rod antenna peak gain is a function of rod length *RL* at the design frequency [20]. For a chosen dielectric thickness, the gain increases as the length of rod increases. The parameter *RL* is chosen to obtain optimum gain over the desired frequency range. Simulated antenna radiation efficiency with and without considering losses are compared in Fig. 2*a*. Antenna radiation efficiency without considering dielectric and metallic losses is close to 95%. Metallic sidewalls are filled up with copper, metallic sheet thickness is considered to be 17 µm. Antenna efficiency including all losses is about 85% over 60 GHz frequency.

The radiation efficiency plot in Fig. 2*a* includes the input GCPW to SIW transition. The design of transition is difficult in this case because the SIW line width is 1.6 mm. As the wider SIW width, second-order modes are generated inside the transition. The scattering parameters experience

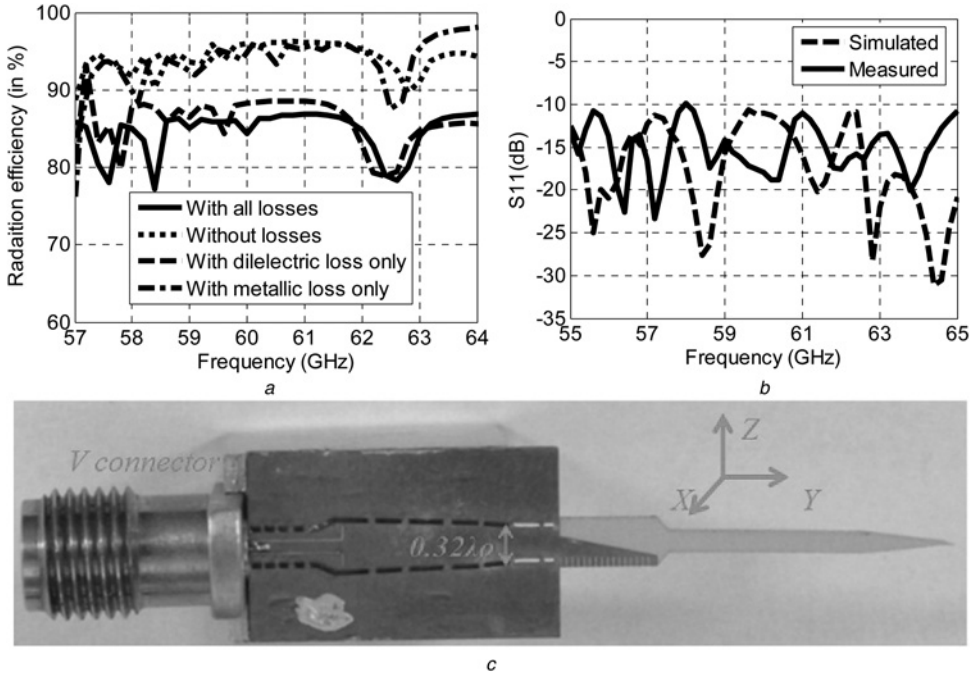

Fig. 2 *Simulated antenna radiation efficiency with and without considering losses*

a Simulated radiation efficiency (with and without considering metallic and dielectric losses) of the final prototype including the input transition
b Simulated and measured reflection coefficient of the dielectric rod antenna
c Manufactured prototype of the rod antenna

dip at 58 and 62.4 GHz. The transition affects the antenna input matching; hence, the radiation efficiency plot has also dips at 58.2 and 62.5 GHz. The input transition is the main cause for the poor efficiency at these two frequencies. The peak gain is reduced and pattern is not symmetrical at these two frequency points, since the power leakage occurs at these two frequency points.

2.3 Antenna cross-pol and SLLs

Antenna cross-pol and SLL as a function of substrate thickness are studied in [25]. It is concluded that, as substrate thickness increases from 10 to 40 mil, cross-pol level as well as SLLs increase. As thickness increases, fields are becoming loosely bounded inside the substrate dielectric, so the polarisation purity is reduced. For 10 mil thickness, the cross-pol exhibits less than −29.35 dB and the worst side-lobe points to −26 dB. Finally, the antenna thickness is considered as 25 mil for the fabricated prototype.

2.4 Measured antenna impedance and radiation pattern bandwidth

The rod antenna of interest is manufactured by using a simple low-cost fabrication process available in our Poly-Grames Research Center. Measured and simulated reflection coefficient magnitudes are compared in Fig. 2*b*. The antenna presents $|S11| \leq -10$ dB from 55 to 65 GHz. Input connector frequency response behaviour seems to affect the shape of the measured reflection coefficient. The experimental prototype of the rod antenna is shown in Fig. 2*c*. *V*-connector is used to measure the input matching (with Anritsu 3739C vector network analyzer) and radiation pattern of the antenna. The total length of the fabricated antenna is $4\lambda_o$ excluding the length of feed waveguide and transition.

Far field antenna pattern is measured in our MI technology anechoic chamber. The rod antenna is placed as receiver and a horn antenna is set as transmitter. The radiation pattern is measured from 57 to 64 GHz at an interval of 0.5 GHz frequency and 2° of interval for gain patterns. Fig. 3 compares simulated and measured radiation patterns in *E*- and *H*-planes at three different frequency points, namely 57, 60 and 64 GHz. Simulated and measured results for co-pol and cross-polarisation levels are also shown in the same figure. Both results are well in agreement and a similar behaviour is observed for all the remaining frequency points. This suggests that all consistent characteristics can be obtained for the full frequency range of interest.

The peak gain values are measured to be 11.5, 12.5 and 12.8 dBi at 57 GHz, 60 and 64 GHz, respectively. Antenna HPBW is calculated to be 40° in both *E*- and *H*-plane radiation cut planes. HPBW of the rod antenna is almost a half when compared with the ALTSA alone, because loading with dielectric rod increases the total gain of the combined structure. The worst SLL is measured to be 10.5 dB lower than the maximum peak gain value. This value can be further lowered by decreasing the thickness of dielectric substrate to 10 mil from the chosen 25 mil thickness. The measured cross polarisation is lower than −13 dB in both the planes.

Measured peak gain difference over the bandwidth from 57 to 64 GHz is less than 1.8 dBi, which is critical for broadband applications. Antenna radiation efficiency of 85% is extracted from the measured peak gain and simulated directivity. Efficiency is primarily affected by the dielectric loss of the substrate.

The comparison between the characteristics of substrate-integrated circuits (SICs) family has been made in Table 1. The proposed antenna makes use of a low cost PCB process instead of our MHMIC fabrication process. Dielectric antennas may be fabricated on the same substrate as part of MHMICs and MMICs, resulting in the lowest connection and possible feeding loss. Among the SICs family, SIW technique is being widely used because of its simplicity in design and also easy to manufacture. Bandwidth of mode matching between input microstrip and CPW lines is also relatively wide when compared with substrate-integrated image guide (SIIG) [19] or substrate-integrated non-radiative dielectric (SINRD) guide [20]. When compared with the multi-layer LTCC, the PCB made phased array antenna is less expensive and easy to manufacture.

The antenna array constructed with dielectric rod antennas is able to satisfy link budget that is required for wireless

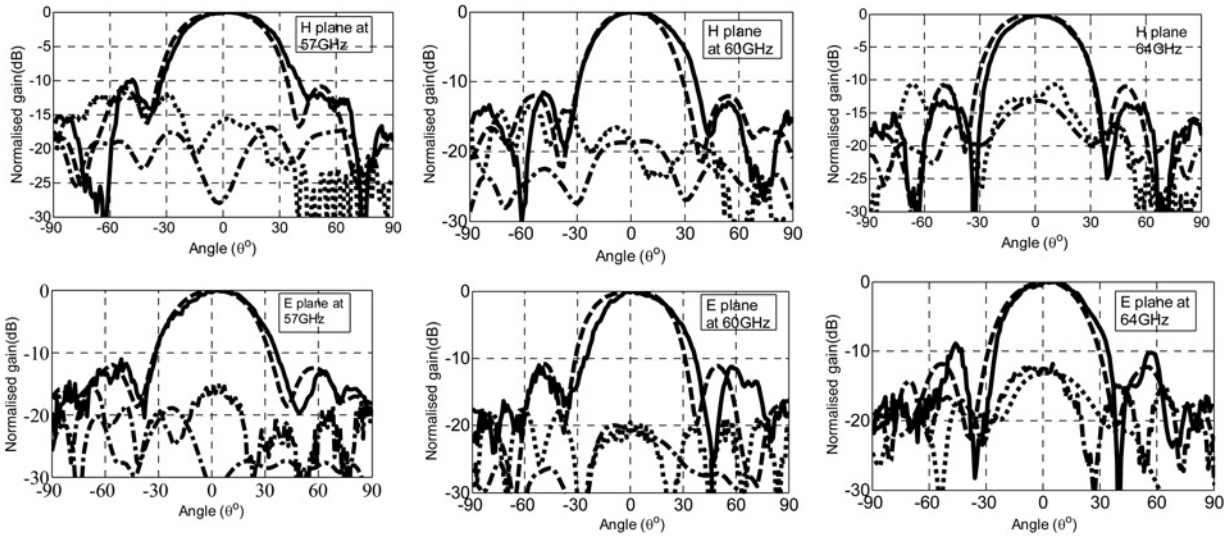

Fig. 3 *E-plane and H-plane co-pol simulation (dash), measurement (solid) and simulated cross-pol pattern (dash-dot) and measured cross-pol pattern (doted) for rod antenna at 57, 60 and 64 GHz*

doi: 10.1049/iet-map.2013.0721

Table 1 Comparison of rod antennas within SICs family

	SIIG	SINRD guide	SIW
fundamental mode	TE_{11}	LSM_{10} and/or LSE_{10}	TE_{10}
transition design	uneasy to integrate with microstrip and CPW structures	uneasy to integrate with microstrip and CPW structures	easy to integrate with microstrip and CPW structures
design complexity	high	high	low
cut-off frequency dependence	substrate thickness	substrate thickness and dielectric width	waveguide width only
useful for frequency range	limited lower frequency use for because of unacceptable leakage and radiation at discontinuities	for *W*-band and beyond	from low GHz applications and above
fabrication complexity	moderate	limitation on substrate thickness	easy
bandwidth of fundamental mode	<20%	<20%	≤50%
remarks	limited use because SIIG open waveguide structure contributes to radiation loss	limited use because SINRD fundamental mode bandwidth may be narrow	widely used

gigabit-per-second communications, and also support beam-forming antenna systems operating at millimetre-wave frequencies. Dielectric rod antennas can also support small footprint designs, which may be of paramount importance for 1D or 2D space-based antenna arrays. On the other hand, phased antenna array and RF front-end can be integrated into a single low-cost package realised with a standard production process. Furthermore, the concept of dielectric rod antenna can be extended to implement on high permittivity silicon substrate for full-scaled semiconductor integrated circuits design. Although antenna performance is generally limited by the dielectric properties of silicon, an antenna designed on such a high permittivity can readily be integrated with the silicon-based platform [13, 14]. Simulated and measured results are compared with validate the proposed concept. Among the SICs family, SIW feeding is also easy to integrate with the active circuitry of the system. SIW feeding rod antennas can be used to implement high gain linearly polarised planar arrays [25].

3 1D scan phased array antenna performance

The dielectric rod antenna discussed above, is used as radiating element to implement 1D scan planar phased array system. Butler matrix based on *H*-plane coupler was proposed to scan directional beam in four fixed directions [26]. The BFN prototype is shown in Fig. 4*a*. The simulated phase and amplitude distributions in the BFN are close to the expected theoretical values. The linear phase gradient at the input of array has four beam forming states, namely +45°, −135°, −45° and +135° for four input ports *P*1–*P*4, respectively, and the amplitude distribution is uniform for all the input ports. Experimental prototype of the phased array antenna is shown in Fig. 4*b*.

The simulated and measured radiation patterns in the azimuth plane for four input ports are shown in Figs. 4*c* and *d*. When the input port is changed from P1 to P4, outgoing beam directions are simulated at four fixed directions as −45°, −10°, +10°, +45° and measured at

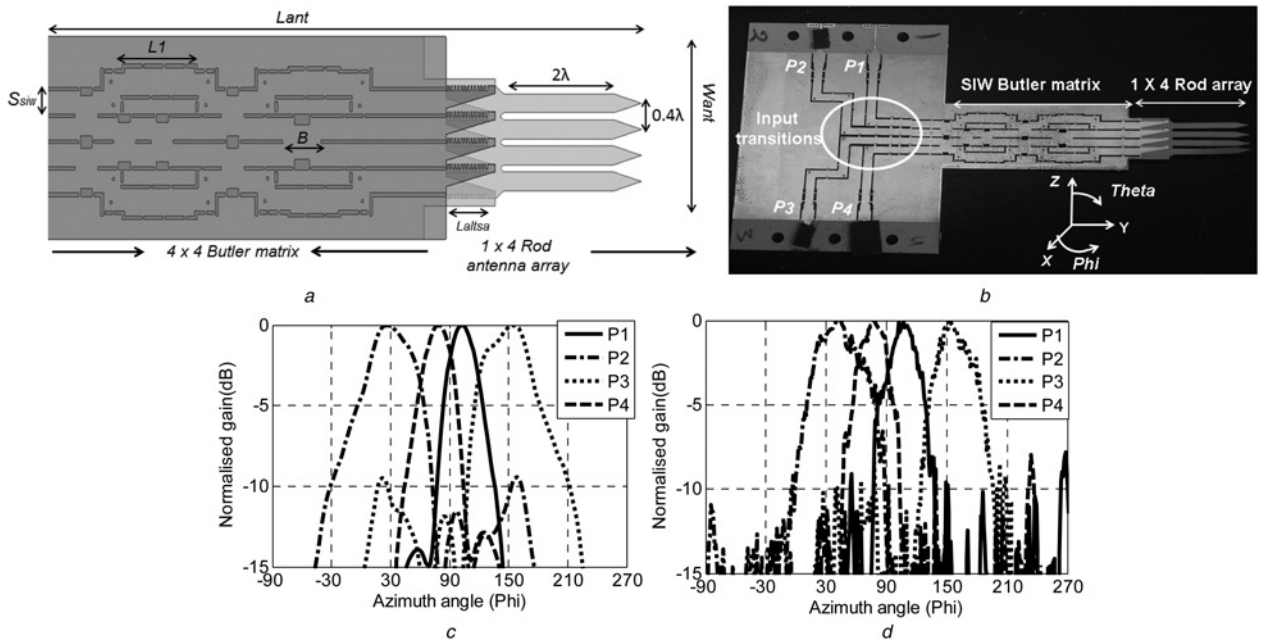

Fig. 4 *1D scan phased array antenna*

a Simulated model ($S_{siw} = 1.57$, $L_1 = 6.58$, $L_{altsa} = 4.5$, $L_{ant} = 56$, $W_{ant} = 14$ and $B = 3.46$, where all dimensions are in mm)
b Fabricated prototype, azimuth plane radiation pattern at 60 GHz frequency
c Simulated
d Measured for four input ports *P*1–*P*4 (where *P* = port number)

−46°, −12°, +12° and +47°, respectively. The comparison between the simulated and measured beam directions is in a good agreement. The HPBW for +135° phase shift is close to 50° and for +45° phase shift is close to 30° at 60 GHz. The phased array has a constant beam direction for each input port when frequency is changed from 59 to 62 GHz. This is because phase dispersion in the BFN is minimised and antenna impedance is matched over a broadband frequency range. The beam pointing error is measured as 5° between the simulated and measured results. Over the 60 GHz frequency band of interest, the measured gain for port 1, port 2, port 3 and port 4 is 14.5 dBi, 12.2 dBi, 12.3 dBi and 14.5 dB, respectively. The rod antenna gain is a function of the dielectric rod length. The 1D phased array antenna is designed on a 10 mil thickness substrate. The rod antenna element length is set to be 2λ so that single element has a wider HPBW and also a better mechanical stability. The single element has 10.5 dBi peak gain at 60 GHz and 1 dB gain difference between lower and higher operating frequency. The phased array is constructed by using the combined structure of BFN and 1 × 4 rod antenna array. The measured gain of the 1D phased array includes the losses of the BFN, and input transitions. The measured average peak gain value is 13 dBi whereas the expected directivity is about 16.5 dBi. The metallic and dielectric losses of substrate decrease the peak gain value by 3.5 dB. For the end user applications, the feeding network loss can be compensated by integrating low-noise/power amplifier in the receiver/transmitter front-end.

4 2D scan phased array antenna performance

In this section, phase shifting network and antenna array architectures are described in detail. The phased array components are designed and fabricated on Rogers 3006 substrate.

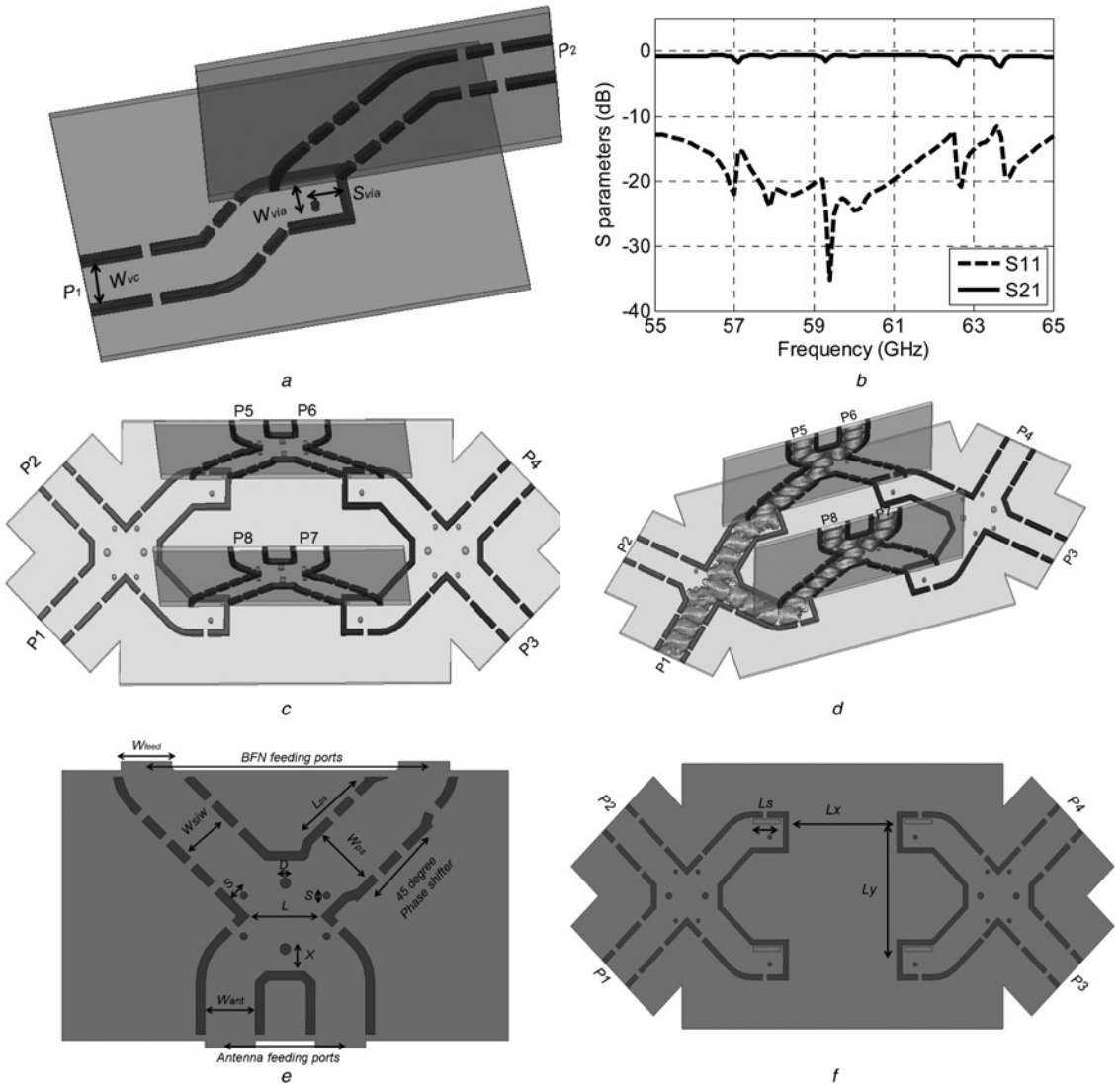

Fig. 5 *Principle is adopted in the design of a vertical interconnect*

a Proposed vertical interconnect ($W_{vc} = 1.7$ mm, $S_{via} = 0.92$ mm and $W_{via} = 2.3$ mm)
b Frequency response
c BFN 3D architecture
d BFN field distribution inside the integrated waveguide topology when fed from port 1, BFN
e Vertical guide part (where $W_{siw} = 1.7$ $W_{feed} = 1.7$, $W_{ant} = 1.7$, $S = 0.76$, $D = 0.4$, $L = 2.4$, $X = 0.76$, $L_{ps} = 2.1$ and $W_{ps} = 2.1$, where all dimensions are in mm)
f Horizontal guide part ($L_s = 1.7$, $L_x = 7.2$ and $L_y = 7.2$, P = port number where all dimensions are in mm)

doi: 10.1049/iet-map.2013.0721

4.1 BFN design

The horizontal and vertical waveguides were connected by using vertical interconnects to build 3D antennas and phased array systems [23]. Similar principle is adopted in the design of a vertical interconnect as shown in Fig. 5*a*, and used to implement a space saving feeding network. The S-parameters as a function of frequency are shown in Fig. 5*b*. Magnitude of transmission coefficient (|*S*21|) is found to be greater than −1 dB and magnitude of reflection coefficient (|*S*11|) is less than −20 dB over the frequency band from 57 to 64 GHz. The metallic post placed on the feeding transmission line improves the matching performance of the vertical interconnect.

The vertical interconnect is used as a basic building block to implement eight port phase shifting network. The cruciform coupler proposed in [27] is used as main coupling unit to implement the BFN. Figs. 5*c* and *d* depict the proposed 3D BFN. When fed from port *P*1 on the feed guide, field is smoothly coupled to the vertical guide and uniformly distributed to the output ports with 45° phase gradient. Similar performance behaviour is expected for remaining two ports, because of the symmetry of BFN. Butler matrix operation principle is obtained with four cruciform couplers and two 45° fixed phase shifters. The Butler matrix special topology is chosen to obtain scanned beams in the azimuth and elevation planes. The eight port network is modified to feed the planar array and to obtain beams in the 2D scan space. The matrix is folded to reduce the size in the azimuth plane and also to feed the elements ports directly. 2D couplers are located on the feed guide and two couplers are on the vertical guide. As shown in Fig. 5*e*, 45° phase shifter is integrated on the vertical guide along the two branches of a coupler. Phase dispersion is reduced by using unequal length and unequal width phase shifter. The four input ports are located on the feed waveguide as shown in Fig. 5*f*.

The amplitude and phase performances of the BFN are shown in Figs. 6*a* and *b*. When fed from port *P*1, magnitude of transmission coefficients (|*S*51, |*S*61|, |*S*71 and |*S*81||) are less than −6.5 dB over the frequency band from 58 to 62 GHz. The phase difference between the output ports is 135°, −45°, 45° and −135° for four input ports *P*1–*P*4, respectively. The phase dispersion is less than 10° over the frequency band from 58 to 62 GHz. Simulated HPBW plotted in Fig. 6*c*, has four clearly defined beam forming directions in the 2D scan space. When the input port is switched from port *P*1 to *P*4, the outgoing beam direction is moving in the azimuth and elevation directions.

4.2 Antenna array design

It is well known that microstrip patch antennas are suitable for implementing compact and light weight phased array antennas. The antenna printed on dielectric substrate is suitable for mass production and can be integrated with any feeding network [28]. Excitation of patch antenna is very

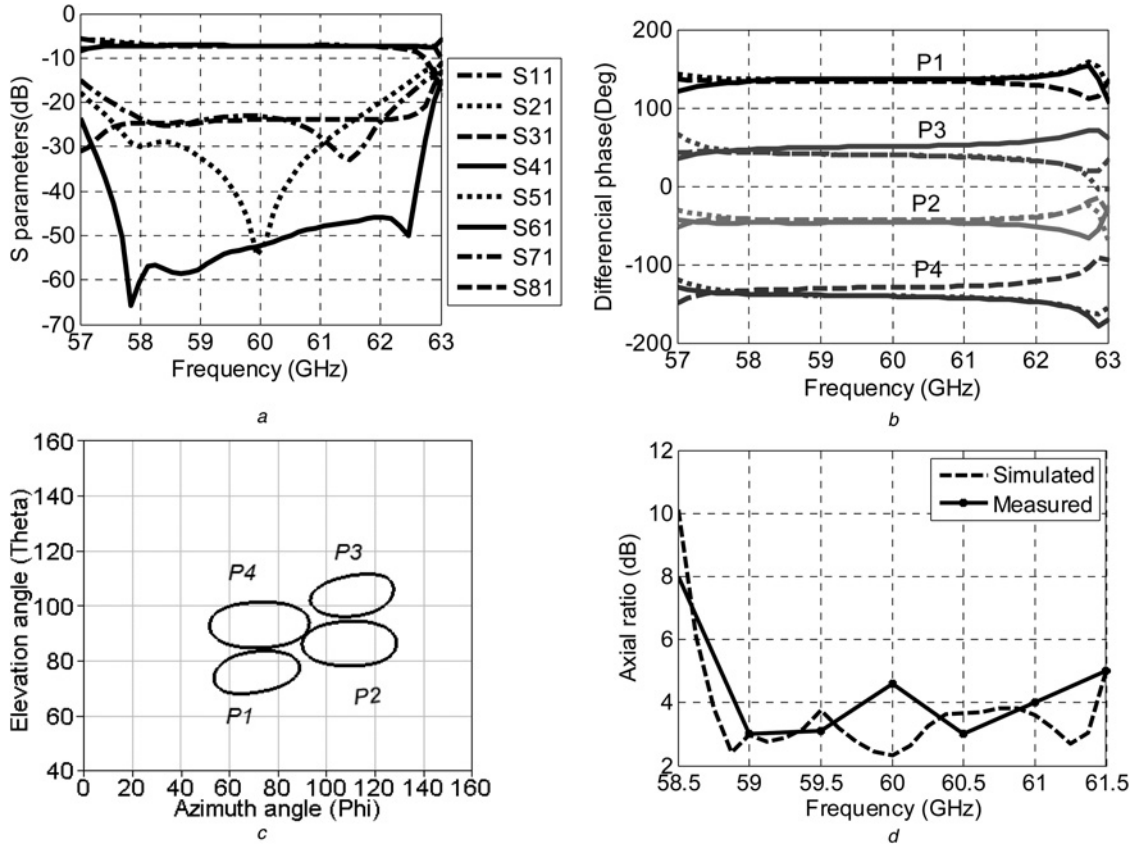

Fig. 6 *BFN*

a Amplitude performance
b Phase gradient as a function of frequency, (solid $\angle S6p - \angle S5p$, dot $\angle S7p - \angle S6p$ and dash $\angle S8p - \angle S7p$, where $p = 1, 2, 3$ and 4
c Simulated HPBW for 2D scan phased array antenna
d Comparison between simulated and measured axial ratio as a function of frequency

critical at millimetre-wave frequency to reduce the radiation leakage and also to obtain good cross-polarisation characteristics. In this work, an aperture coupling method is used for the excitation and slot antenna is used as an excitation source to obtain good cross-polarisation characteristics.

A circularly polarised (CP) radiating element is chosen to construct a radiating aperture [12]. Antenna has unidirectional radiation pattern characteristics and RHCP gain of 7.5 dBc. The radiated beam direction is constant over the frequency band from 58 to 62 GHz. As illustrated in Fig. 7, CP element is used to construct a three-layered antenna array. Feeding layer (Rogers 3006 with $\varepsilon_r = 6.3$, 10 mil thickness) is an SIW transmission line where excitation slots are etched, the second layer (Rogers 5880 with $\varepsilon_r = 2.2$, 31 mil thickness) acts as an SIW cavity and air gap, the third layer (Rogers 3850 with $\varepsilon_r = 2.9$, 1 mil thickness) is antenna layer. The top and bottom metallic planes are connected through metallic filled vias, so that the antenna does not experience any back lobe radiation. The metallic cavities synthesised on the second layer are able to enhance the gain of antenna by suppressing higher order surface modes in the structure. The metallic walls are suppressing unwanted surface modes and also decreasing the mutual coupling between adjacent antenna elements. Each slot is etched at a distance of one quarter wavelength from the edge of a short circuited SIW line, so that maximum source excitation is obtained in the feeding network. CP antenna impedance is matched to cover the frequency band from 58 to 62 GHz. The spacing between antenna elements in *X*- and *Y*-directions is fixed at 0.7λ and 0.8λ, respectively. The radiating aperture is RHCP array with a simulated broadside gain of 13 dBc over the designed frequency band.

4.3 Measured phased array performance

The phased array prototype as shown in Fig. 7*d*, is fabricated in two steps. In the first step, BFN parts are fabricated individually (Rogers 3006 with $\varepsilon_r = 6.3$, 10 mil thickness) and then vertical guide feed sections are inserted into the slots drilled along the horizontal guide. In the second step, the three-layer antenna array is fabricated by using a multi-layer fabrication process and then the BFN output ports are inserted into the slots made on the SIW feeding layer of antenna array. 2D scan phased array impedance and radiation pattern characteristics are measured by using four V-band connectors. Array impedance is matched in the scanned beam direction over the frequency range from 58 to 62 GHz. Antenna far-field radiation pattern characteristics are measured in our compact range MI technology reverberation chamber and a linearly polarised V-band horn antenna is used as a radiating source.

Fig. 8 plots the measured radiation pattern as a function of the azimuth angle (phi). For port 1 to port 4, the maximum gain is measured at an angle of (phi, theta) (70°, 75°), (70°, 95°), (110°, 80°) and (110°, 100°). The simulated and measured beam patterns are compared and a good agreement is obtained for different frequency points. Each directive beam maximum gain is extracted after the calibration with two standard horn antennas. Axial ratio values are extracted from difference gain values of the azimuth and elevation gain patterns. As compared to Fig. 6*d*, the measured axial ratio is less than 4.5 dB over the bandwidth from 58.8 to 61.5 GHz for port P1. The measured axial ratio was extracted from the difference of amplitude received with the horizontal and vertical polarizations. The measured axial ratio values were higher than the simulated values, mainly because of

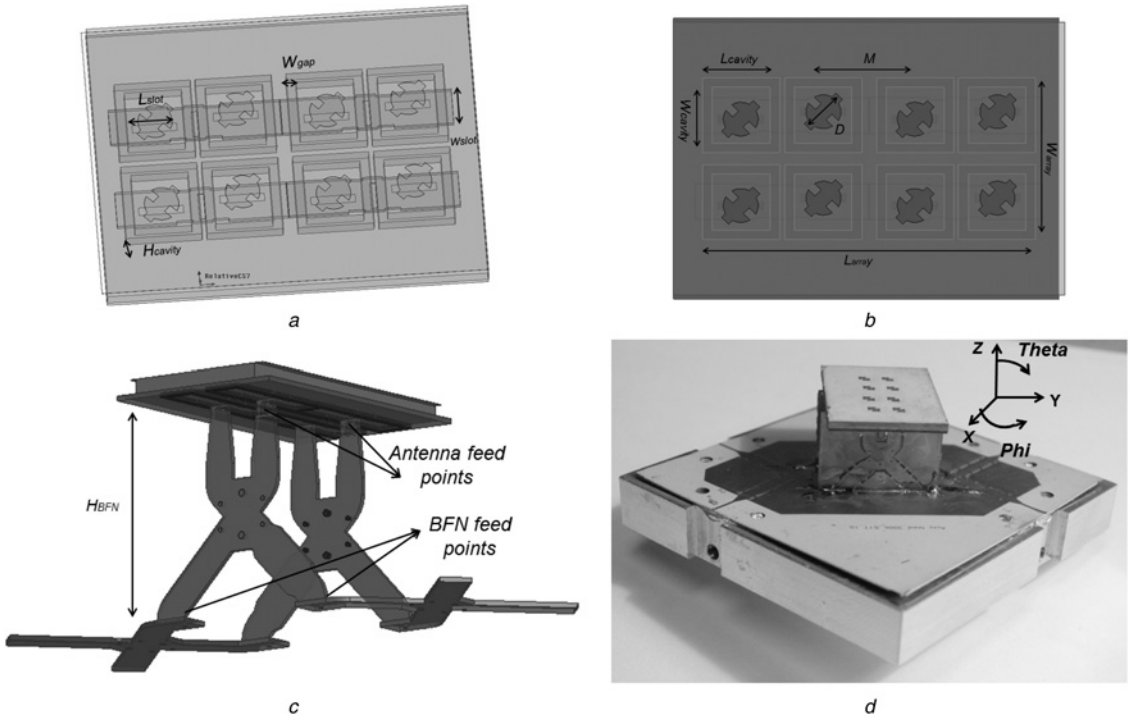

Fig. 7 *Antenna array*

a Transparent view
b Top view, and phased array antenna (where $W_{gap} = 0.3$, $L_{slot} = 1.87$, $W_{slot} = 1.52$, $H_{cavity} = 0.635$, $W_{cavity} = 2.9$, $L_{cavity} = 2.8$, $W_{array} = 8.6$, $D = 1.84$, $M = 4.1$, $L_{array} = 15$ and $H_{BFN} = 11$, where all dimensions are in mm)
c Simulated prototype
d Experimental prototype

doi: 10.1049/iet-map.2013.0721

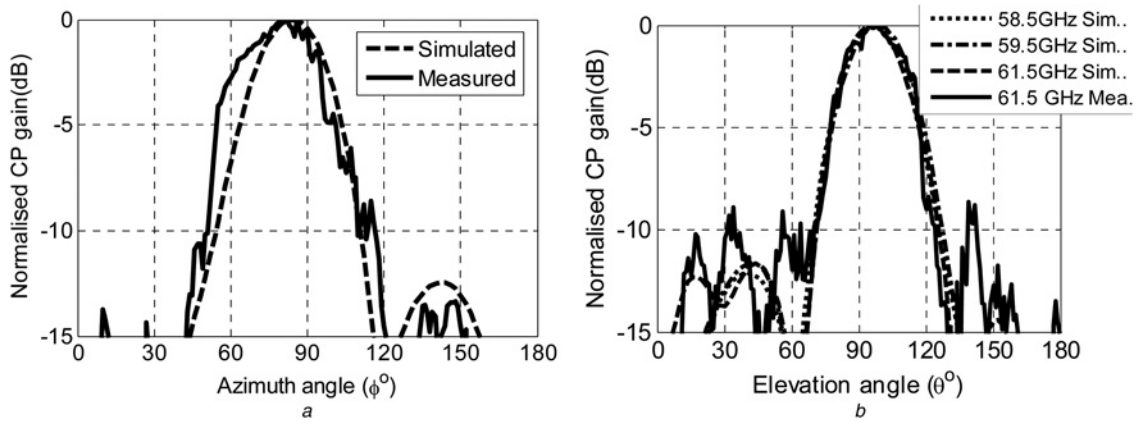

Fig. 8 *2D scan phased array performance at 60 GHz frequency for*
a Port 1 in azimuth plane
b Port 4 in elevation plane

fabrication tolerances and slight misalignment effects in the anechoic chamber. The antenna has a wide azimuth plane HPBW of 38° and a narrow elevation plane HPBW of 18° because the array construction is a rectangular planar array. The BFN phase and amplitude distributions are uniform over the frequency band and the measured SLLs are −8 dB lower than the maximum beam in the scanned direction. As frequency increases, phase dispersion introduced in the BFN increases and subsequently SLL increases. The RHCP phased array peak gain is measured as 12.8 dBc for input ports over the frequency range from 58.5 to 61.5 GHz. The maximum measured beam pointing error is 5° for edge scanned beams. The fabrication tolerances introduced by the laser-perforating machine deviates the outgoing beam direction from the expected beam direction.

5 Conclusion

In this work, a linearly polarised phased array with 1D scanning and a CP phased array with 2D scanning techniques are introduced and experimentally characterised over the 60 GHz frequency range. In the first technique, a class of planar SIW-fed high efficiency dielectric rod antennas is discussed and studied. A 1×4 linear rod antenna array is fed by using a Butler matrix and a complete phased array is integrated in a single layer substrate. The 1D scan phased array is fully planar and has four beam forming states for four inputs. The physical size is $3\lambda \times 12\lambda \times 0.01\lambda$ and each phase steered beam has gain of 13 dBi. In the second technique, 2D scan RHCP phase array antenna implemented by using 2×4 antenna array and folded Butler matrix. The feed network size in the azimuth plane is reduced by using a vertical interconnect and folded in half to feed planar array. The physical size is $6\lambda \times 3\lambda \times 2.2\lambda$ and each phase steered CP beam has gain of 12 dBc. The single polarised (RHCP) phased array performance can be extended to dual polarised (LHCP and RHCP) phased array by using the folded BFN concept.

6 References

1 Mitola, J., Maguire, G.Q.: 'Cognitive radio: making software radios more personal', *IEEE Pers. Commun.*, 1999, **6**, (4), pp. 13–18
2 Hall, P.S., Gardner, P., Faraone, A.: 'Antenna requirements for software defined and cognitive radios'. Proc. IEEE, 2012, vol. 99, pp. 1–9
3 Tawk, Y., Bkassiny, M., El-Howayek, G., *et al.*: 'Reconfigurable front-end antennas for cognitive radio applications', *IET Microw. Antennas Propag.*, 2011, **5**, (8), pp. 985–992
4 Kenington, P.B.: 'Emerging technologies for software radio', *Electron. Commun. Eng. J.*, 1999, **11**, (2), pp. 69–83
5 Balanis, C.A.: 'Antenna theory: analysis and design' (Wiley, New York, 2005, 3rd edn.)
6 Bozzi, M., Georgiadis, A., Wu, K.: 'Review of substrate-integrated waveguide circuits and antennas', *IET Microw. Antennas Propag.*, 2011, **5**, (8), pp. 909–920
7 Guntupalli, A.B., Wu, K.: 'Multi-dimensional scanning multi-beam array antenna fed by integrated waveguide Butler matrix'. IEEE MTT-S Int. Microwave Symp., June 2012, pp. 1–3
8 Cheng, Y.J., Bao, X.Y., Guo, Y.X.: '60-GHz LTCC miniaturized substrate integrated multibeam array antenna with multiple polarizations', *IEEE Trans. Antennas Propag.*, 2013, **61**, (12), pp. 5958–5967
9 Moulder, W.F., Khalil, W., Volakis, J.L.: '60-GHz two-dimensionally scanning array employing wideband planar switched beam network', *IEEE Antennas Wirel. Propag. Lett.*, 2010, **9**, pp. 818–821
10 Guntupalli, A.B., Djerafi, T., Wu, K.: 'Two dimensional scan antenna array fed by the integrated waveguide phase shifter', *IEEE Trans. Antennas Propag.*, 2014, **62**, (3), pp. 1117–1124
11 Guntupalli, A.B., Wu, K.: '60 GHz circularly-polarized smart antenna system for high throughput two-dimensional scan cognitive radio'. IEEE MTT-S Int. Microwave Symp., June 2013, pp. 1–3
12 Guntupalli, A.B., Wu, K.: 'Millimeter-wave phased array antenna for high throughput two-dimensional scan cognitive radio'. IEEE Int. Wireless Symp. (IWS), April 2013, pp. 1–4
13 Gentile, G., Jovanovic, V., Pelk, M.J., *et al.*: 'Silicon-filled rectangular waveguides and frequency scanning antennas for mm-wave integrated systems', *IEEE Trans. Antennas Propag.*, 2013, **61**, (12), pp. 5893–5901
14 Li, D.X., Zhang, Y.P.: 'Integration of array antennas in chip package for 60-GHz radios'. Proc. of the IEEE, 2012, vol. 100, no. 7, pp. 2364–2371
15 Chen, X.-P., Wu, K., Han, L., *et al.*: 'Low-cost high gain planar antenna array for 60-GHz band applications', *IEEE Trans. Antennas Propag.*, 2010, **58**, pp. 2126–2129
16 Leib, M., Vollmer, A., Menzel, W.: 'An Ultra-wideband dielectric rod antenna fed by a planar circular slot', *IEEE Trans. Microw. Theory Tech.*, 2011, **59**, (4), pp. 1082–1089
17 Shiau, Y.: 'Dielectric rod antennas for millimeter-wave integrated circuits', *IEEE Trans. Microw. Theory Tech.*, 1976, **24**, (11), pp. 869–872
18 Chen, C.-C., Ramarao, K., Lee, R.: 'A new ultra wide-bandwidth dielectric-rod antenna for ground-penetrating radar applications', *IEEE Trans. Antennas Propag.*, 2003, **51**, (3), pp. 371–377
19 Patrovsky, A., Wu, K.: '94-GHz planar dielectric rod antenna with substrate integrated image guide (SIIG) feeding', *IEEE Antennas Wirel. Propag. Lett.*, 2006, **5**, pp. 435–437
20 Ghassemi, N., Wu, K.: 'Planar dielectric rod antenna for gigabyte chip-to-chip communication', *IEEE Trans. Antennas Propag.*, 2012, **60**, (10), pp. 4924–4928
21 Kazemi, R., Fathy, A.E., Sadeghzadeh, R.A.: 'Dielectric rod antenna array with substrate integrated waveguide planar feed network for wideband applications', *IEEE Trans. Antennas Propag.*, 2012, **60**, (3), pp. 1312–1319
22 Sun, M., Qing, X.Q., Chen, Z.N.: '60-GHz antipodal Fermi antenna on PCB'. Proc. Fifth European Conf. Antennas Propagation, April 2011, pp. 3109–3112

23 Guntupalli, A.B., Wu, K.: 'Polarization-agile millimeter wave antenna arrays'. Asia-Pacific Microwave Conf. (APMC), December 2012, pp. 148–150
24 Ghassemi, N., Wu, K.: 'Planar high-gain dielectric-loaded antipodal linearly tapered slot antenna for E- and W-Band gigabyte point-to-point wireless services', *IEEE Trans. Antennas Propag.*, 2013, **61**, (4), pp. 1747–1755
25 Guntupalli, A.B., Wu, K.: 'Milli-meter wave antenna arrays for high performance Radar/Radio Systems at 60 GHz'. Int. Symp. Antennas Propag. (ISAP), October 2013, pp. 589–592
26 He, F.F., Wu, K., Hong, W., *et al.*: 'Low-cost 60-GHz smart antenna receiver subsystem based on substrate integrated waveguide technology', *IEEE Trans. Microw. Theory Tech.*, 2012, **60**, (4), pp. 1156–1165
27 Djerafi, T., Wu, K.: 'Super-compact substrate integrated waveguide cruciform directional coupler', *IEEE Microw. Wirel. Compon. Lett.*, 2007, **17**, (11), pp. 757–759
28 Chang, K. (Ed.): 'Handbook of microwave and optical components' (Wiley, New York, 1989)

doi: 10.1049/iet-map.2013.0721